Supporting Information

Luu et al. 10.1073/pnas.1010331108

SI Text

Section 1. ***Spherule geometry.*** Consider an initially disk-shaped patch of radius r_d, height h, volume $V = \pi {r_d}^{2*}h$, and apical surface area $A_d = \pi {r_d}^2$ (Fig. 1*L*). As the patch becomes spherical, the volume of the sphere with radius r_s is conserved, i.e., $\pi {r_d}^{2*}h = (4/3)\pi {r_s}^3$, and the apical area is now $A_s = 4\pi {r_s}^2$. To completely move all basolateral surface to the inside of the spherule, the apical surface area must expand by $A_s/A_d = 3h/r_s$. When sphere size is further increased, the required expansion of the apical surface diminishes, to vanish at $r_s = 3h$ (Fig. 1*L*). Above $r_s = 3h$ excess available apical surface should result in nonspherical shapes. However, folded patches become wrinkled below this size.

We propose that elasticity resists cell shape change during the rounding up of epithelial patches (1), leading to wrinkling of explants with $r_s < 3h$. (Explants showed no sign of surface tension on their exposed apical sides, as discussed in the main text; thus wrinkling was not due to the Rayleigh capillary instability of liquid cylinders.) Anticlinal and oblique cell divisions also relieve strain by producing less elongated daughter cells. However, these division modes are rare at gastrula stages, and their effect will develop very slowly compared with explant folding, allowing wrinkling to dominate.

To accurately model the transition to wrinkling would seem to require the application of nonlinear elasticity, but simple considerations can convey the basic idea. Essentially, we model the onset of wrinkling as the splitting of a rounded explant into two equal-sized smaller ones of the same total volume (Fig. 1*H*) and propose that this occurs at a critical radius to reduce strain energy. When explants round into spherules, cells increase their apical surface areas while simultaneously bending and increasing their heights (Fig. 1*L*). For larger explants, both the apical expansion and the bending are less severe; thus the resistance to the formation of larger spherules that leads to wrinkling must be due to the height strain.

We use a simple network of springs to model the epithelium (Fig. S2) (2, 3). Strain energy originates in the stretching of the springs. Bending energy is implicitly included and the total strain energy could equivalently be expressed in the form used by Helfrich (4), in which the bending energy is explicit, but the present approach is simpler.

In three dimensions, each cell is associated with two apical springs and one height spring. The strain energy of the apical springs is

$$U_a = 2 \cdot \frac{1}{2}\,\kappa\varepsilon_a^2, \qquad \text{[S1]}$$

and the strain energy of the height spring is

$$U_h = \frac{1}{2}\,\kappa\varepsilon_h^2. \qquad \text{[S2]}$$

In the above, ε_a is linear apical strain, ε_h is height strain, and κ is a stiffness (assumed equal for both springs).

We estimate the equilibrium positions of the springs from images of epithelia cut away on three sides from the inner ectoderm under conditions that eliminate basal side adhesion (one example is in Fig. 2*I*). The equilibrium height is $h_0 = 28 \pm 6.5$ μm ($n = 6$).

By conservation of volume between a flat and a curled epithelium (Fig. 2*I*), $A_d h = A_{1/2} h_0$, where $A_{1/2}$ is the area of the midplane of the curled epithelium (halfway between apical and basal sides). The area of the apical side of the curled epithelium is

$$A_0 = A_{1/2}\,\frac{R - h_0/2}{R}, \qquad \text{[S3]}$$

where $R = 34 \pm 3.8$ μm ($n = 6$) is the radius of curvature of the curled epithelium at its midplane (Fig. 2*I*).

Spherical wrinkling. The linear apical strain in a spherule is approximately

$$\varepsilon_a = \frac{1}{2}\left(\frac{A_s}{A_0} - 1\right) = \frac{1}{2}\left(\frac{A_s}{A_d}\,\frac{A_d}{A_{1/2}}\,\frac{A_{1/2}}{A_0} - 1\right) = \frac{1}{2}\left(\frac{4\pi r_s^2}{\pi r^2}\,\frac{h_0}{h}\,\frac{R}{R - h_0/2} - 1\right) = \frac{1}{2}\left(\frac{3h}{r_s}\,\frac{h_0}{h}\,\frac{R}{R - h_0/2} - 1\right), \qquad \text{[S4]}$$

where r_d is the radius of the initial flat disk (sheet), and r_s the radius of the spherule. Assuming interior cells (Fig. 1*C*) occupy a radius $\rho \sim 15$ μm (Fig. 1*C*) in the spherule, the height strain is

$$\varepsilon_h = \frac{r_s - \rho}{h_0} - 1. \qquad \text{[S5]}$$

The total strain energy per cell, normalized by κ, is

$$\frac{U}{\kappa} = \frac{1}{4}\left(\frac{3h_0}{r_s}\,\frac{R}{R - h_0/2} - 1\right)^2 + \frac{1}{2}\left(\frac{r_s - \rho}{h_0} - 1\right)^2. \qquad \text{[S6]}$$

We model the wrinkled shape as two attached spheres, each of radius $2^{-1/3} r_s$ for conservation of volume. The strain energy for the wrinkled shape is

$$\frac{U_w}{\kappa} = \frac{1}{4}\left(\frac{3h_0}{2^{-1/3} r_s}\,\frac{R}{R - h_0/2} - 1\right)^2 + \frac{1}{2}\left(\frac{2^{-1/3} r_s - \rho}{h_0} - 1\right)^2. \qquad \text{[S7]}$$

The condition for wrinkling to be energetically favorable is $U_w < U$. This condition occurs when $r_s > 69$ μm.

Cylindrical wrinkling. Larger wrinkled explants approximately take the shape of multiply bent cylinders. A similar model to that described above can be applied to roughly estimate the cylinder radius r_c that minimizes the total strain energy per cell:

$$\frac{U}{\kappa} = \frac{1}{4}\left(\frac{2h_0}{r_c}\,\frac{R}{R - h_0/2} - 1\right)^2 + \frac{1}{2}\left(\frac{r_c - \rho}{h_0} - 1\right)^2. \qquad \text{[S8]}$$

U is numerically minimized at $r_c = 53$ μm for the parameter values given above.

Section 2. ***Condition for spreading.*** Spreading of epithelium on other tissue is different from spreading of liquids or mesenchyme because the epithelium has effective surface tension on only one side (the basolateral surface). However, the derivation of a rule for spreading closely follows that of the analogous rule for liquids (5).

The work of cohesion of a liquid is defined as the work required, per unit area, to separate an infinite volume of the liquid into two parts (5). If the process creates two new liquid surfaces where there were none before, then the work of cohesion of liquid 1 is equal to the change in surface energy per unit area:

$$W_{11} = 2\gamma_1. \quad \textbf{[S9]}$$

If instead volumes of two different liquids 1 and 2 are separated, then the process destroys a 1–2 interface and creates surfaces of liquids 1 and 2; hence

$$W_{12} = \gamma_1 + \gamma_2 - \gamma_{12}. \quad \textbf{[S10]}$$

W_{12} is the strength of the bonds that held unit areas of liquids 1 and 2 together. The interfacial tension $\gamma_{12} \geq 0$; otherwise the 1–2 surface is energetically unfavorable and the liquids mix.

We assume that increasing the exposed basal surface by unfolding or spreading of an epithelial sheet (Fig. 3*A*) requires work analogous to that needed to increase the surface area of cell aggregates; thus

$$\gamma_e = W_{ee}/2. \quad \textbf{[S11]}$$

When placed on an aggregate of mesenchymal cells with surface tension

$$\gamma_m = W_{mm}/2, \quad \textbf{[S12]}$$

the interfacial tension is

$$\gamma_{em} = W_{mm}/2 + W_{ee}/2 - W_{em}. \quad \textbf{[S13]}$$

As for two mesenchymal aggregates, if, hypothetically, $\gamma_{em} < 0$, then mixing is energetically favored; for an epithelium, the sheet-like structure imposed by the subapical junctions would presumably limit mixing to fingering of the epithelium into the mesenchyme.

Suppose an epithelium partially surrounds a mesenchymal aggregate. If the epithelium unfolds or spreads such that a unit area of epithelium–epithelium basolateral contact is lost, then the epithelium can advance to cover two more units of aggregate surface (Fig. 3*A*). The energy change is therefore $S = W_{ee} - 2W_{em} = 2(\gamma_{em} - \gamma_m)$. Whether the epithelium advances or recedes depends on the sign of the spreading parameter S. Unlike for a liquid, partial spreading is not possible due to surface forces alone.

Balance of surface and elastic forces. When epithelium spreads on mesenchymal tissue, spreading is resisted by the elasticity of the epithelium. We assume that cell rearrangement (Fig. S5*C*) relieves any elastic stress in the mesenchymal tissue. We treat the epithelium as a 2D isotropic circular elastic sheet subjected to a radial pressure representing the interfacial tension difference. Defining a stiffness k by

$$\varepsilon_r = \frac{1}{k}(\sigma_r - \nu\,\sigma_\theta), \quad \textbf{[S14]}$$

where ε_r is radial strain, σ_r is radial stress, σ_θ is angular stress, and ν is Poisson's ratio, and applying a solution for an elastic cylinder (6) with $\nu = 0.5$ for a soft material, we obtain Eq. **1** in the text. Because spreading occurs at a constant curvature of the epithelium (the curvature of the surface of the underlying spherical mesenchymal aggregate, Fig. 3 *F–H*), there is no force due to bending energy.

Combining rules for interfacial tensions. Knowing the value of the interfacial tension is critical for the prediction of spreading, but measuring it directly is often not possible, and values are based on assumptions. If both cell types express the same adhesion molecules, adhesion strength between pairs of cells that differ in adhesiveness may correspond to that between two cells with the lower adhesiveness (7).This assumption suggests $W_{em} = \min(W_{ee}, W_{mm})$; i.e.,

$$\gamma_{em} = |\gamma_e - \gamma_m| \quad \textbf{[S15]}$$

(Fig. 3*B*), known as Antonow's rule in the study of liquid surface tensions (8). The predicted condition for spreading is then $|\gamma_e - \gamma_m| < \gamma_m$ or $\gamma_e < 2\gamma_m$. Alternatively, one may assume that adhesion between cells obeys a geometric mean (Berthelot) combining rule (8, 9) (strictly justified for van der Waals forces, but not for cell adhesion), resulting in an interfacial tension of

$$\gamma_{em} = \gamma_e + \gamma_m - 2(\gamma_e\gamma_m)^{1/2}. \quad \textbf{[S16]}$$

In this case, the condition for spreading is $\gamma_e < 4\gamma_m$ (Fig. 3*B*).

Section 3. ***Measurement of tissue surface tensions.*** Tissue surface tensions were measured with axisymmetric drop shape analysis (ADSA). A tissue explant allowed to reach equilibrium becomes drop shaped, reflecting a compromise between tissue surface tension (which seeks a sphere) and gravity (which seeks a flat puddle). The drop shape is described mathematically by the Laplace equation of capillarity,

$$P_0 + \Delta\rho g z = \gamma\left(\frac{1}{R_1} + \frac{1}{R_2}\right), \quad \textbf{[S17]}$$

where P_0 is the pressure difference across the aggregate apex, $\Delta\rho$ is the density difference between the aggregate and the immersion medium, g is gravitational acceleration, z is the vertical distance from the apex, γ is the tissue surface tension, and R_i are the radii of curvature of the aggregate profile.

ADSA (10) is a computer program that numerically integrates the Laplace equation to generate theoretical drop shapes for different hypothetical surface tensions, optimizing the surface tension to find the theoretical shape that best fits an experimental profile (from an image of a drop). The best fit identifies the operative surface tension. The density difference $\Delta\rho$ must be measured separately.

ADSA was recently adapted for use with tissue explants (11), by introducing more robust methods for image analysis and initial value finding in the numerical procedure, to handle the irregularity of cell aggregate profiles (compared with those of liquid drops).

Accurate measurement of γ requires that different values of γ produce discernibly different aggregate shapes. This is not the case for large γ, when surface tension overwhelms gravity and the aggregate becomes spherical. As seen in Fig. S6, accurate measurements can be obtained for $\gamma < \sim 1$ mJ/m^2, which is the case for all tissues in this study. Thus, measurement of tissue surface tension simply consisted of imaging equilibrated shapes of explants (in side view) and fitting the aggregate-medium profiles using the ADSA program. Details including density measurement are available elsewhere (11).

Measurement of interfacial tensions. When coated with excess epithelium (i.e., enough that the epithelium fully coated the aggregates without stretching), round aggregates flattened until an equilibrium was reached (Fig. 3*K*). Aggregates were then fixed and bisected (Fig. 3*J*). Assuming that further flattening was prevented by interfacial tension, Laplacian profiles were fitted to the boundaries between inner cells and epithelium (11). Due to strong flattening, fits were of modest quality. Nonetheless, because γ_{em} was very small compared with γ_m, and only their difference is important in Eqs. **2** and **3** of the main text, to a good approximation we used $\gamma_{em} \sim 0$, giving $\gamma_e \sim \gamma_m$.

Measurement of epithelial explant dimensions. Spherule images were processed by an edge detector (Canny) in Matlab and the edge was fitted to an ellipse. Outlying edge points were eliminated and the remaining edge points were newly fitted. Parameters were varied until fits were visually suitable. The ellipse axis perpendicular to the image plane was assumed to be equal to the shorter

of the (usually similar) visible axes. The equivalent radius was calculated for a sphere of the same volume (Fig. 1*J*).

For spreading and recoiling patches, the boundary between epithelium and substrate layer was manually drawn (Microsoft Paint) on the first image in each time lapse. Edge detection was used to find the boundary in subsequent images, discarding edge points that were far from any edges in the previous two images. Noise was further reduced by ordering edge points by their polar angle and eliminating points with large radial jumps from their neighbors. Image processing parameters were adjusted by visual inspection to ensure reasonable fits throughout each time lapse. The area of the polygon defined by the ordered edge points was calculated, and the patch radius was defined as the radius of a circle with the same area. Radii were least-squares fitted to dying exponentials in time (Fig. S5*B*). For all analyses, results (e.g., time constants) typically changed $\leq \sim 20\%$ when the manually set parameters were varied in a reasonable range.

1. Derganc J, Svetina S, Zeks B (2009) Equilibrium mechanics of monolayered epithelium. *J Theor Biol* 260:333–339.
2. Safran SA (1999) Curvature elasticity of thin films. *Adv Phys* 48:395–448.
3. Petrov AG, Bivas I (1984) Elastic and flexoelectric aspects of out-of-plane fluctuations in biological and model membranes. *Prog Surf Sci* 16:389–512.
4. Helfrich W (1973) Elastic properties of lipid bilayers: Theory and possible experiments. *Z Naturforsch C* 28:693–703.
5. Israelachvili JN (1991) *Intermolecular and Surface Forces* (Academic, London).
6. Crandall SH, Dahl NC, Lardner TJ (1999) *An Introduction to the Mechanics of Solids* (McGraw-Hill, New York), , 2nd Ed, p 296.
7. Krieg M, et al. (2008) Tensile forces govern germ-layer organization in zebrafish. *Nat Cell Biol* 10:429–436.
8. Kwok DY, Neumann AW (1999) Contact angle measurement and contact angle interpretation. *Adv Colloid Interface Sci* 81:167–249.
9. Steinberg MS (1978) In *Specificity of Embryological Interactions (Receptors and Recognition, Series B)*, ed Garrod DR (Chapman & Hall, London), Vol 4, pp 99–129.
10. Rotenberg Y, Boruvka L, Neumann AW (1983) Determination of surface tension and contact angle from the shapes of axisymmetric fluid interfaces. *J Colloid Interface Sci* 93:169–183.
11. David R, Ninomiya H, Winklbauer R, Neumann AW (2009) Tissue surface tension measurement by rigorous axisymmetric drop shape analysis. *Colloids Surf B Biointerfaces* 72:236–240.

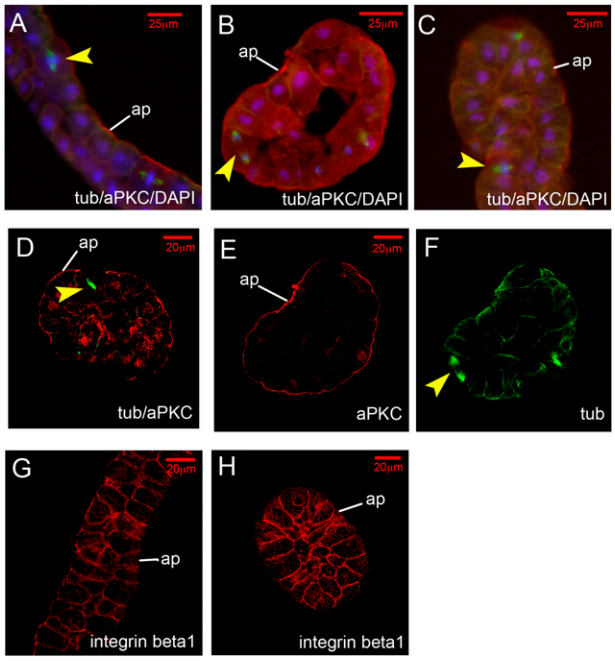

Fig. S1. Immunostaining of sectioned ectoderm and epithelial explants. (*A*–*C*) Ectoderm or epithelial explants stained with aPKC antibody (red) to indicate apical surface (ap), tubulin antibody (green) showing microtubules, and DAPI to reveal nuclei or chromosomes (blue); viewed in fluorescence microscope. (*D*–*F*) Epithelial explants stained for aPKC (red) and tubulin (green), viewed in a confocal microscope. (*E* and *F*) Same explant as in *B* in red and green channels, respectively. Orientation of mitotic spindles (yellow arrowhead): *A*, *B*, and *F*, parallel to apical surface; *C* and *D*, perpendicular or oblique to surface. (*G* and *H*) Staining of ectoderm (*G*) or epithelial explant (*H*) with an integrin antibody shows lack of integrinβ1 on apical (ap) surfaces and expression on all other membranes.

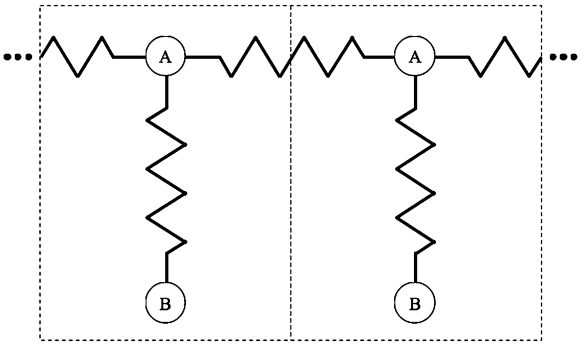

Fig. S2. Cross-section of spring model for the mechanics of epithelial folding. Two more apical springs extend into and out of the page, respectively, at each point A. Dotted lines delineate cells. A, apical side; B, basal side.

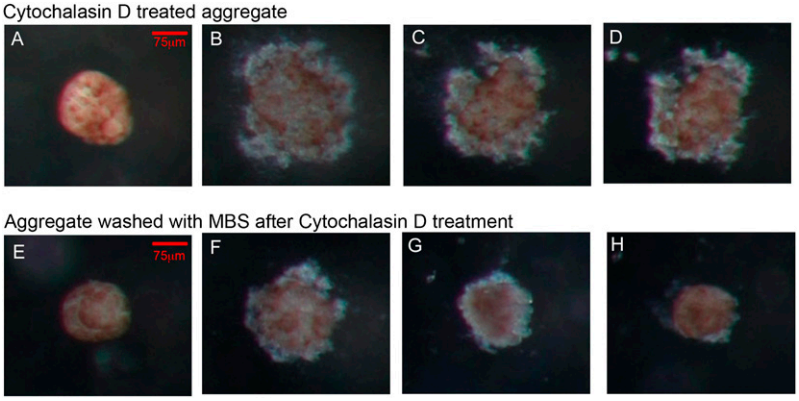

Fig. S3. Effect of 0.5 μM cytochalasin D on elasticity. In preliminary experiments that explored a range of concentrations (0.2–10 μM), 0.5 μM was found to be effective in our experiments without strongly affecting explant integrity. (*A–D*) Continuous incubation in cytochalasin D: rounded epithelial explant at the onset of cytochalasin treatment, before compression (*A*), after 1 h of compression before (*B*) and directly after (*C*) lifting of coverslip, and 1 h after removing coverslip (*D*). Four of five explants behaved as shown. (*E–H*) Pulse treatment with cytochalasin D: rounded explant at onset of cytochalasin incubation, before compression (*E*); after 1 h of cytochalasin D treatment followed by 1 h of washing in MBS, directly before (*F*) and after (*G*) lifting of coverslip; and 1 h later (*H*). Five of five explants showed this behavior. A second independent experiment gave similar results.

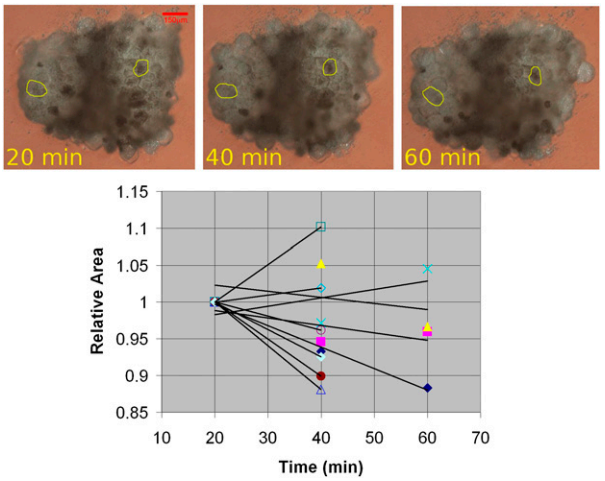

Fig. S4. An explanted epithelial patch can be cultured in Ca^{2+}- and Mg^{2+}-free MBS for prolonged times without dissociation into single cells (in contrast to EDTA-containing buffer). Explants are uneven and cells tend to move slowly in and out of focus. Nevertheless, the areas of 10 cells were followed from $t = 20$ min to either $t = 40$ min or $t = 60$ min. Apical areas were fit to straight lines in time; the average of the fitted slopes was not significantly different from zero ($P = 0.20$); i.e., there was no significant overall change in cell area.

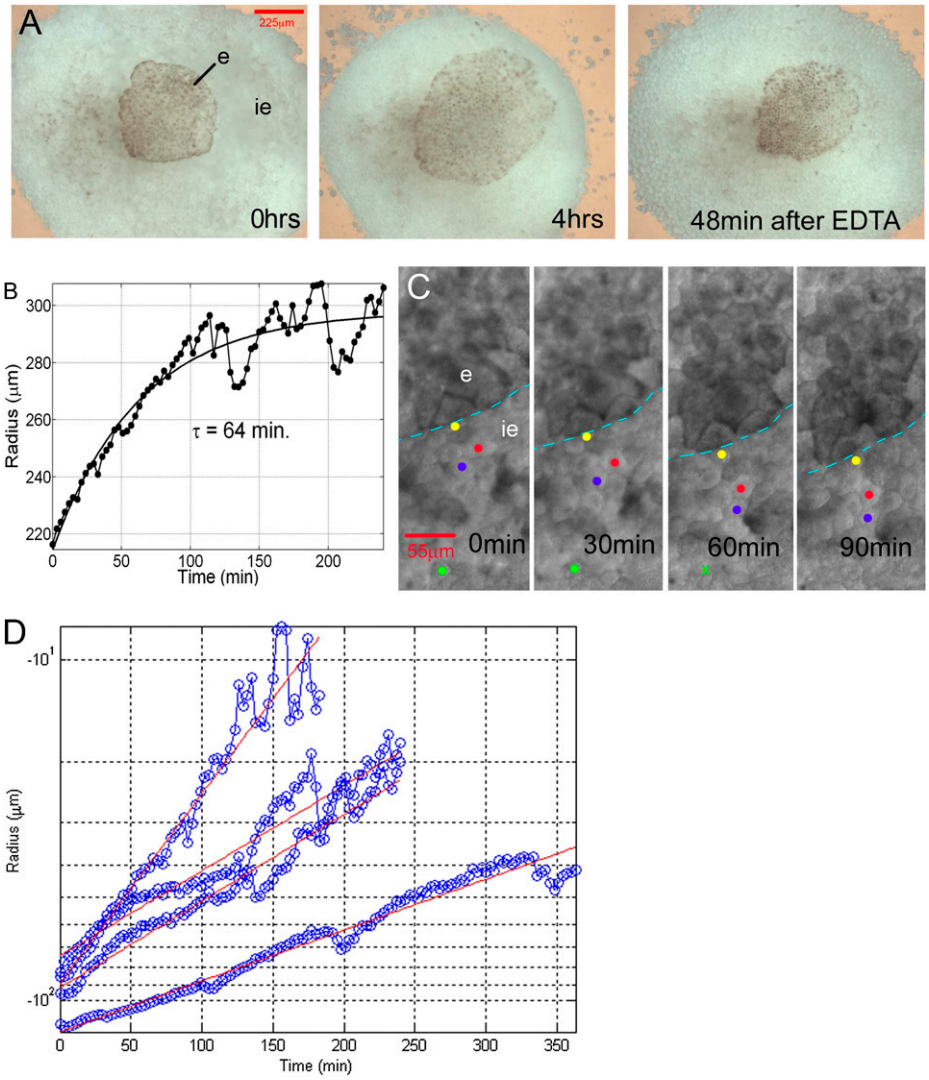

Fig. S5. Spreading of ectodermal epithelial patches on inner ectoderm layer. (*A*) Frames from time-lapse recordings of epithelial patch (center, brown) on inner ectoderm (white) at beginning and end of spreading and after subsequent EDTA treatment. (*B*) Time course of spreading; τ, time constant. (*C*) Spreading occurred by intercalation of inner cells; inner cells ahead of the advancing front of epithelial cells moved with the epithelium rather than being overtaken by it. (*D*) Exponential spreading. The logarithm of the equivalent radius as a function of time is shown for four explants (blue). The curves do not deviate systematically from the straight lines fitted to them (red). Differences in slopes reflect natural variation (Table S1).

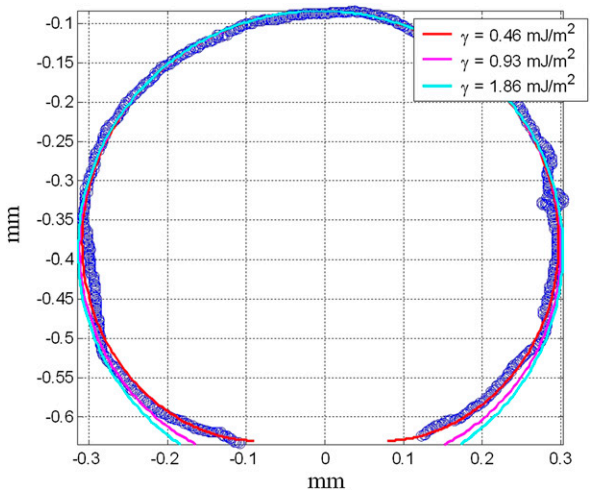

Fig. S6. Fit of an explanted aggregate to a Laplacian curve, with alternate superimposed curves for different hypothetical surface tensions, showing that it is possible to distinguish the correct from the incorrect surface tension for $\gamma < \sim 1$ mJ/m^2.

Table S1. Spreading of epithelial patches on inner ectodermal cells

Patch	Initial radius, μm	Spread radius, μm	Retracted radius, μm	Time constant for spreading, min
a	276	355	—	291
b	219	306	—	64
c	250	270	—	28
d	255	320	276	174
e	249	321	235	78
f	226	301	214	171
g	240	289	—	53
h	228	329	—	—
i	240	282	—	—

Table S2. Spreading of ectodermal epithelium on different substrates

Tissue	Spread	Attached	Retracted	Sum
Ectoderm	23	0	0	23
Chordamesoderm	26	4	3	33
Prechordal mesoderm	13	5	3	21
Leading edge mesendoderm	0	6	14	20
Endoderm	0	1	11	12